EXPERIMENTAL VERIFICATION OF PHYSICAL MODELS FOR A SOLID PHASE

Rudolf Brepta, Josef Hégr, Petr Hora

The results obtained by measuring eigenfrequencies of solid bodies are presented. The measurements were carried out by electroacoustical impulse method. The bodies being investigated were represented by a cylindrical wave guide, thin disc, thin ring and thick ring, each of the bodies being made of structural steel. The results of measurements were compared with those obtained through theoretical methods developed earlier. Maximum differences between experiments and theory are of the order of a few per cent.

LIST OF SYMBOLS

a	radius
b	width of a ring
c	phase velocity
c_0	bar velocity
c_3	velocity of a dilatation wave in two-dimensional continuum
d	diameter
f	frequency
h	thickness of a ring, thickness of a disc
j	quadratic radius of inertia
l	length
m	integer
n	integer
r_1	radius of a disc
A	constant
B	constant
D	diameter
E	Young's modulus
L	length
R	mean radius of a ring
$\alpha_s^{(n)}, \beta_s$	eigenvalue

μ Poisson's ratio
ϱ density
Δ eigenvalues difference
Λ wave length

1. INTRODUCTION

The paper gives comprehensive results of experimental verification of properties of physical models (of continuum) for a solid phase. The electroacoustic impulse method was used to find the initial region of a line spectrum of natural frequencies of the body or set of bodies being investigated. By comparing the natural frequencies obtained in this way with theoretical values we can verify the validity or the limits of validity of the physical model employed to calculate the frequencies.

To define the behaviour of the bodies under investigation, the model of a linear elastic continuum for small deformations was used. By modelling the bodies made of steel the model of continuum may be employed up to the frequencies of the order of 100 MHz. The domain of frequencies being investigated was limited from above by the frequencies 20 – 30 kHz, which is far below the limit frequency.

On the one hand, we verified quite exact models (in the sense of the linear theory of small deformations), on the other hand, simplified one-dimensional models were investigated, such as, for instance, the model of a curved bar. For these, so-called, approximate theories in particular, the impulse method is very efficient because it can quickly yield the boundaries for the usefulness of these models.

The bodies being investigated are as follows:

a) cylindrical rod with a circular cross section (cylindrical wave guide),
b) thin circular disc (plane state of stress),
c) thin circular ring,
d) thick circular ring.

Paper [3] shows the first results obtained by one of the authors of this paper by measuring longitudinal and transversal vibrations of a cylindrical rod with a finite cross section. The experimental results proved to be in a very good agreement with theoretical values of frequencies obtained through the Pochhammer solution, see [5], namely for the first dispersion branch. The measurements proved that at least a part of frequencies of longitudinal vibrations, pertaining to the second and third dispersion branch, can be determined through the given apparatus.

The frequencies of extensional vibrations of a thin disc are presented in papers [2] and [5].

Frequency equations of extensional vibrations of a thin and thick ring are presented in [1]. These equations follow from the simple theory of a curved bar, which was improved through corrections concerning rotation of elements of the ring, its transverse cross section, and the shear due to a shear force.

The block diagram of the measuring arrangement is shown in Fig. 1, where

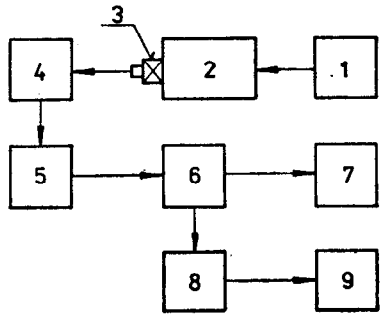

Fig. 1.

1 – source of pulses of the force
2 – measured model
3 – acceleration pickup KD 91/118
4 – pickup amplifier RFT SDM 132
5 – digital recorder of short-run processes B & K 7502
6 – narrow-band frequency analyzer B & K 2031
7 – level recorder B & K 2305
8 – interface
9 – tape punch B & K 6301.

A particular description of the electroacoustic impulse method of measuring is given in [4], and also in [3]. The stress pulse in the measured model was aroused by an impact of a steel ball suspended on a thin thread. As a result of the fact that no considerable fall of amplitudes of natural frequencies was encountered in measured spectra, the stress pulse generated in this way can be supposed to converge to the Dirac pulse. Through the agency of the stress pulse the measured models theoretically experience vibrations at all frequencies. The time response of the stress pulse was trapped by the acceleration pickup, and processed by the frequency analyzer. In this way the spectrum of all frequencies of the model was obtained. All the spectra presented in this paper were obtained by the linear averaging of 32 spectra of the respective measuring. By averaging the results, disturbing influences were suppressed. By carrying out the measurement the frequency analyzer was equipped with a weight filtr with a linear characteristic ("FLAT"). The accuracy of measuring the frequencies on a spectral analyzer is given by the frequency range being chosen on the analyzer. By measuring the cylindrical wave guide, this accuracy was 75 Hz, 62·5 Hz and 50 Hz. By measuring a thin disc and a thin ring the frequencies were red with the accuracy 50 Hz. By measuring a thick ring the accuracy ranged from 1·25 Hz to 50 Hz.

2.1 Longitudinal vibrations

In a rod of finite length L, the measured value of frequency of longitudinal vibrations, f_n, allows the phase velocity of the wave, c, to be obtained from the formula

$$c_n = \frac{2f_nL}{n}, \tag{2-1}$$

where n is an integer ($n = 1, 2, 3, \ldots$). Hence, it is evident that from this formula we get a number of discrete values of velocity c_n. In a thin bar, when a wave length $\Lambda = 2L/n$ is by one order greater than its transverse dimension, the velocity $c \doteq c_0$ is steady, independent of frequency. In a bar, whose transverse dimension cannot be neglected, velocity c is a function of frequency, and geometrical dispersion is encountered.

The result of measuring is represented by a spectrum of natural longitudinal vibrations of the wave guide (Fig. 2.)*). Employing the frequency analyzer, we can from

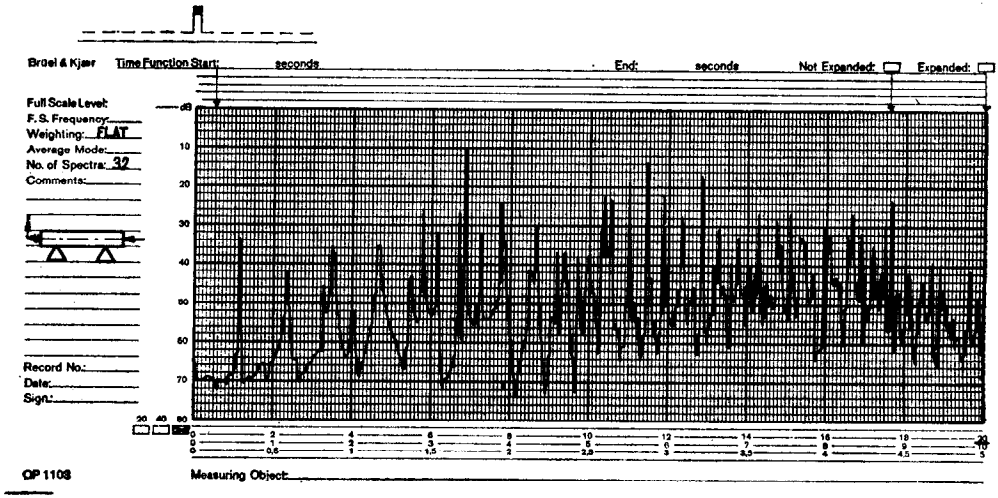

Fig . 2.

the spectrum determine natural frequencies of the wave guide, f_n, and then, from formula (2-1), we can calculate velocities c_n. Now we carry out the scaling of velocities

*) It is impossible to arouse the stress disturbance such which only allows a rotationally symmetrical longitudinal vibration to be generated. Transversal waves too are always propagating in the model, hence, the response in Fig. 2 and next figures shows very small amplitudes of these parasitic oscillations too.

c_n and frequencies f_n, employing the formulae

$$c_{Nn} = \frac{c_n}{c_0}, \tag{2-2}$$

$$f_{Nn} = \frac{a \cdot f_n}{c_n} = \frac{a}{\Lambda_n}, \tag{2-3}$$

and then we can plot the measured points of dispersion curve. In relations (2-2), (2-3), the subscript N stands for the scaling values, a is radius of the rod. The dimensions of the rod are as follows: $L = 2{\cdot}165$ m; $\varnothing d = 2a = 0{\cdot}29$ m.

The measuring of points of the basic branch of the dispersion curve was relatively simple. From the measured spectrum of longitudinal oscillations (see, for instance, Fig. 2) we select the natural frequencies f_n with greatest amplitudes, then, on substitu-

Table I

n	f_n [Hz]	c_n [m/s]	f_{Nn}	c_{Nn}
1	1 200	5 200	0·033	1·000
2	2 400	5 200	0·067	1·000
3	3 600	5 200	0·100	1·000
4	4 750	5 140	0·134	0·990
5	5 850	5 070	0·167	0·975
6	6 900	4 980	0·201	0·958
7	7 850	4 860	0·234	0·935
8	8 700	4710	0·268	0·906
9	9 450	4 550	0·301	0·875
10	10 050	4 350	0·335	0·838
11	10 600	4 170	0·368	0·803
12	11 050	3 990	0·402	0·767
13	11 500	3 830	0·435	0·737
14	11 950	3 700	0·469	0·711
15	12 400	3 580	0·502	0·689
16	12 900	3 490	0·536	0·672
17	13 350	3 400	0·569	0·654
18	13 850	3 330	0·603	0·641
19	14 350	3 270	0·636	0·629
20	14 900	3 230	0·670	0·621
21	15 400	3 180	0·703	0·611
22	16 000	3 150	0·737	0·606
23	16 600	3 130	0·770	0·601
24	17 200	3 100	0·804	0·597
25	17 850	3 090	0·837	0·595
26	18 500	3 080	0·871	0·593
27	19 200	3 080	0·904	0·593

ting these frequencies in relation (2-1) we get velocities c_n, and eventually, we carry out the scaling through relations (2-2) and (2-3). The values obtained by measuring and calculation are presented in Tab. I. Tab. II shows the comparison of the points of the basic branch of the dispersion curve, obtained by measuring a circular rod of a finite length, with the points calculated by the Pochhammer equation (see, for instance, equation (2-1) in paper [3]), which defines the dispersion response in circular rods of infinite length. For the scaling frequency f_{Nn}, the scaling velocity c_{Nn} is presented, calculated from the measured values, and, further, Tab. 2 shows the theoretical value of the scaling velocity c_{NnT}, calculated from the Pochhammer equation for the same value of f_{Nn}. The measured rod being made of structural carbon steel. The Poisson ratio of the steel is supposed to be equal to 0·29. This value was substituted into the Pochhammer equation. Moreover, Tab. II shows an absolute value of a percentage difference Δ between c_{Nn} and c_{NnT}.

Table II

n	f_{Nn}	c_{Nn}	c_{NnT}	$\lvert\Delta\rvert$ [%]
1	0·033	1·000	0·999	0·1
2	0·067	1·000	0·996	0·4
3	0·100	1·000	0·991	0·9
4	0·134	0·990	0·983	0·7
5	0·167	0·975	0·972	0·3
6	0·201	0·958	0·956	0·2
7	0·234	0·935	0·934	0·1
8	0·268	0·906	0·906	0·0
9	0·301	0·875	0·871	0·5
10	0·335	0·838	0·834	0·5
11	0·368	0·803	0·798	0·6
12	0·402	0·767	0·764	0·4
13	0·435	0·737	0·734	0·4
14	0·469	0·711	0·709	0·3
15	0·502	0·689	0·688	0·1
16	0·536	0·672	0·670	0·3
17	0·569	0·654	0·655	0·2
18	0·603	0·641	0·643	0·3
19	0·636	0·629	0·633	0·6
20	0·670	0·621	0·624	0·5
21	0·703	0·611	0·617	1·0
22	0·737	0·606	0·611	0·8
23	0·770	0·601	0·606	0·8
24	0·804	0·597	0·601	0·7
25	0·837	0·595	0·598	0·5
26	0·871	0·593	0·595	0·3
27	0·904	0·593	0·592	0·2

The boundary conditions on the faces of a rod of finite length are somewhat different from those in cross sections of an infinite rod. However, the results of measuring show that the difference is small, and it quickly dies away in a short distance from the faces of the rod.

The measuring of points of the second and third branch of the dispersion curve was somewhat more difficult. This is due to the fact that for the rod in question the respective natural frequencies are encountered in the frequency band above 10 kHz. In this band the rod experiences a great number of natural frequencies whose amplitudes are relatively small (see Fig. 2). Hence, it was necessary to select those natural frequencies f_n, referring to the points of the second and third branch of the dispersion

Table III

n	f_n [Hz]	c_n [m/s]	f_{Nn}	c_{Nn}
1	13 200	57 160	0·033	11·002
2	12 900	27 930	0·067	5·376
3	12 700	18 330	0·100	3·528
4	12 600	13 640	0·134	2·626
5	12 550	10 910	0·167	2·100
6	12 600	9 090	0·201	1·750
7	12 875	7 960	0·234	1·533
8	13 200	7 140	0·268	1·375
9	13 812	6 650	0·301	1·279
10	14 600	6 320	0·335	1·217
11	15 500	6 100	0·368	1·174
12	16 350	5 900	0·402	1·136
13	17 250	5 750	0·435	1·106
14	18 400	5 690	0·469	1·095
15	19 400	5 600	0·502	1·078
16	20 400	5 520	0·536	1·063
17	21 375	5 440	0·569	1·048
18	22 125	5 320	0·603	1·025
19	22 875	5 210	0·636	1·003
20	23 600	5 110	0·670	0·984
21	24 250	5 000	0·703	0·962
22	24 900	4 900	0·737	0·943
23	25 500	4 800	0·770	0·924
24	26 000	4 690	0·804	0·903
25	26 625	4 610	0·837	0·888
26	21 125	4 520	0·871	0·870
27	27 700	4 440	0·904	0·855
28	28 250	4 370	0·938	0·841
29	28 875	4 310	0·971	0·830
30	29 375	4 240	1·005	0·816

curve. The selection was carried out in such a way that all natural frequencies obtained by measuring were stored in memory of the computer. For the cylindrical wave guide in question the natural frequencies had to be read also in the band above 20 kHz as, below this frequency, only a relatively small number of the respective frequencies was encountered. Accordingly, for some measurements, the frequency range of the spectral analyzer B & K 2031 was extended through the digital recorder of short-run processes B & K 7502. This approach made it possible to read the natural frequencies of a cylindrical wave guide up to the value 32 kHz. Further, we inserted the exact points of the second and third branch of the dispersion curve into the memory of the computer. These points were obtained by solving the Pochhammer equation for a rod of an infinite length. Among these exact points, the computer approximated the dispersion curves via short line segments, and calculated theoretical natural frequencies f_n referring to the second and third dispersion branch. From the set of the measured frequencies the computer selected those converging to the theoretical values.

Table IV

n	f_n [Hz]	c_n [m/s]	f_{Nn}	c_{Nn}
1	14 200	61 490	0·033	11·836
2	14 800	32 040	0·067	6·168
3	15 200	21 940	0·100	4·223
4	15 900	17 210	0·134	3·313
5	16 600	14 380	0·167	2·767
6	17 200	12 410	0·201	2·389
7	17 875	11 060	0·234	2·128
8	18 500	10 010	0·268	1·927
9	19 250	9 260	0·301	1·783
10	20 000	8 660	0·335	1·667
11	20 800	8 190	0·368	1·576
12	21 625	7 800	0·402	1·502
13	22 562	7 510	0·435	1·447
14	23 200	7 180	0·469	1·381
15	23 875	6 890	0·502	1·327
16	24 875	6 730	0·536	1·296
17	25 500	6 500	0·569	1·250
18	26 125	6 280	0·603	1·210
19	27 125	6 180	0·636	1·190
20	28 250	6 120	0·670	1·177
21	29 100	6 000	0·703	1·155
22	30 000	5 900	0·737	1·137
23	31 000	5 840	0·770	1·123
24	32 000	5 770	0·804	1·111

The measured values of eigenfrequencies f_n, and the respective calculated phase velocities c_n for the second branch of the dispersion curve are presented in Tab. III. Further, the table shows the scaling frequencies f_{Nn} and scaling velocites c_{Nn} calculated from relations (2-3) and (2-2).

Tab. IV shows the measured eigenfrequencies f_n, calculated phase velocities c_n, scaling frequencies f_{Nn}, and scaling velocities c_{Nn} for the third branch of the dispersion curve of longitudinal waves.

The absolute values of the percentage differences Δ between the points of the second and third branch of the dispersion curve obtained by measuring a rod of finite length, and the points referring to the theoretical curve of the second and third dispersion branch of a rod of an infinite length, are set up in Tab. V and Tab. VI.

Table V

n	f_{Nn}	c_{Nn}	c_{NnT}	$\lvert\Delta\rvert$ [%]
1	0·033	11·002	11·075	0·7
2	0·067	5·376	5·401	0·5
3	0·100	3·528	3·531	0·1
4	0·134	2·626	2·615	0·4
5	0·167	2·100	2·083	0·4
6	0·201	1·750	1·746	0·2
7	0·234	1·533	1·523	0·7
8	0·268	1·375	1·375	0·0
9	0·301	1·279	1·277	0·2
10	0·335	1·217	1·213	0·3
11	0·368	1·174	1·170	0·3
12	0·402	1·136	1·139	0·3
13	0·435	1·106	1·116	0·9
14	0·469	1·095	1·097	0·2
15	0·502	1·078	1·079	0·1
16	0·536	1·063	1·061	0·2
17	0·569	1·048	1·043	0·5
18	0·603	1·025	1·024	0·1
19	0·636	1·003	1·004	0·1
20	0·670	0·984	0·984	0·0
21	0·703	0·962	0·963	0·1
22	0·737	0·943	0·942	0·1
23	0·770	0·924	0·923	0·1
24	0·804	0·903	0·904	0·1
25	0·837	0·888	0·886	0·2
26	0·871	0·870	0·870	0·0
27	0·904	0·855	0·854	0·1
28	0·938	0·841	0·840	0·1
29	0·971	0·830	0·826	0·5
30	1·005	0·816	0·814	0·2

Table VI

n	f_{Nn}	c_{Nn}	c_{NnT}	$\lvert\Delta\rvert$ [%]
1	0·033	11·836	11·816	0·2
2	0·067	6·168	6·122	0·8
3	0·100	4·223	4·239	0·4
4	0·134	3·313	3·306	0·2
5	0·167	2·767	2·751	0·6
6	0·201	2·389	2·387	0·1
7	0·234	2·128	2·129	0·0
8	0·268	1·927	1·937	0·5
9	0·301	1·783	1·789	0·3
10	0·335	1·667	1·672	0·3
11	0·368	1·576	1·576	0·0
12	0·402	1·502	1·496	0·4
13	0·435	1·447	1·429	1·3
14	0·469	1·381	1·372	0·7
15	0·502	1·327	1·322	0·4
16	0·536	1·296	1·281	1·2
17	0·569	1·250	1·245	0·4
18	0·603	1·210	1·216	0·5
19	0·636	1·190	1·192	0·2
20	0·670	1·177	1·172	0·4
21	0·703	1·155	1·154	0·1
22	0·737	1·137	1·139	0·2
23	0·770	1·123	1·125	0·2
24	0·804	1·111	1·111	0·0

Here, for the scaling frequency f_{Nn}, the scaling velocity c_{Nn} calculated from the measured values is presented. Further, the theoretical value of the scaled velocity c_{NnT} is set up, calculated from the Pochhammer equation for the same value f_{Nn}.

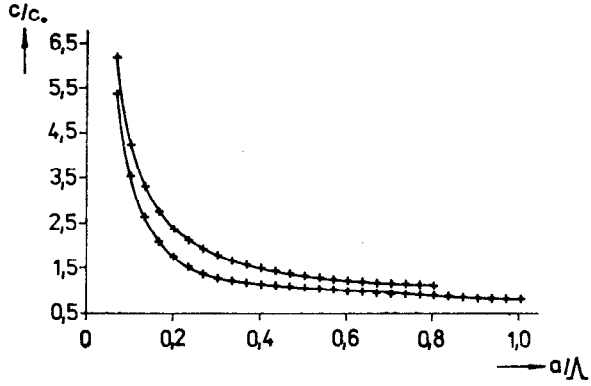

Fig. 3a.

Fig. 3a shows the second and third dispersion branch obtained by measuring. As a result of a finite length of the rod it is impossible to measure arbitrary values of points on dispersion curves, only a discrete set of points may be obtained. The particular points obtained by measuring are marked by crosses in Fig. 3a. For comparison this figure also shows the second and third branch of the dispersion curve of a circular rod of infinite length. To avoid the coalescence of both curves, the values are plotted only up to the value of the scaled velocity $c_N = c/c_0 = 6{\cdot}5$, i.e., the first points obtained by measuring ($n = 1$) are left out.

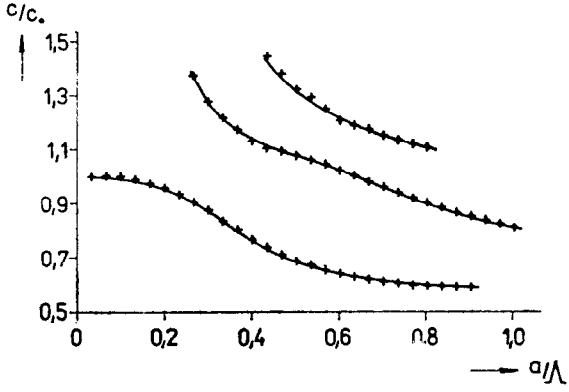

Fig. 3b.

Fig. 3b shows all three dispersion branches. For comparison, this figure also shows the first three branches of dispersion curves of a rod of infinite length with circular cross section. For a good overview, Fig. 3b shows the scaling velocities only up to the value $c_N = c/c_0 = 1{\cdot}5$.

2.2 Flexural vibrations

In practical measurements the attention was only focused on the points of the basic branch of the dispersion curve of flexural waves (transversal vibrations). The procedure of the measuring and the processing of the results are similar to those used by measuring longitudinal waves. In view of the fact that a great number of natural frequencies with various amplitudes were obtained, it was necessary to determine the respective frequencies pertaining to the basic dispersion branch (similarly as in the case of the second and third branch of longitudinal waves) by employing a special selecting method.

In paper [4] it was proved that for a rod of infinite length the dependence of velocity c_n upon the value a/Λ_n can be approximated by the relation

$$\frac{c_n}{c_0} \doteq A\left(1 - e^{a/\Lambda_n B}\right), \tag{2-4}$$

which can very well substitute the curve obtained by the Pochhammer solution. For

$\mu = 0{\cdot}29$, the value of $A = 0{\cdot}5736$; $B = 0{\cdot}1581$. A maximum error of the approximation is 0·97%.

Employing relation (2-4), we calculated the theoretical values of flexural frequencies f_n which are, to compare the results, given in Tab. VII.

Table VII

n	f_n [Hz]
1	5
2	132
3	697
4	1 870
5	3 677
6	6 039
7	8 834
8	11 949
9	15 358
10	19 075

The real flexural frequencies f_n obtained by measuring, and the respective phase velocities c_n calculated from these frequencies are presented in Tab. VIII. Further,

Table VIII

n	f_n [Hz]	f_{Nn}	c_n [m/s]	c_{Nn}
1	5	0·007	110	0·021
2	130	0·034	560	0·107
3	700	0·084	1 210	0·234
4	1 900	0·150	1 840	0·353
5	3 600	0·234	2 230	0·430
6	5 850	0·336	2 520	0·486
7	8 800	0·457	2 790	0·537
8	11 850	0·597	2 880	0·554
9	15 350	0·756	2 940	0·566
10	19 700	0·934	3 060	0·589

this table sets up the scaling frequencies f_{Nn} and scaling velocities c_{Nn} obtained by relations (2-3), (2-2).

Further (similarly as in Section 2.1), we carried out the comparison between the measured points of the basic branch of the dispersion curve of flexural waves in

a rod of finite length, and the points obtained by the Pochhammer equation for flexural waves in a rod of infinite length.

The absolute values of percentage differences Δ between the points obtained by measuring the dispersion curve of flexural waves, and the points obtained theoretically are set up in Tab. IX. For the scaling frequencies f_{Nn}, the table shows the scaling velocities c_{Nn} calculated from the values obtained by measuring, and the theoretical values of scaling velocities c_{NnT}, obtained by the Pochhammer equation for flexural waves (see, for instance, eqs. (1.6)–(4) in paper [4]). The symbol Δ stands for the percentage differences between the values c_{Nn} and c_{NnT}.

Table IX

n	f_{Nn}	c_{Nn}	c_{NnT}	$\lvert\Delta\rvert$ [%]
1	0·007	0·021	0·021	0·0
2	0·034	0·107	0·104	2·8
3	0·084	0·234	0·235	0·4
4	0·150	0·353	0·355	0·6
5	0·234	0·430	0·443	3·0
6	0·336	0·486	0·501	3·1
7	0·457	0·537	0·537	0·0
8	0·597	0·554	0·558	0·7
9	0·756	0·566	0·570	2·5
10	0·934	0·589	0·575	2·4

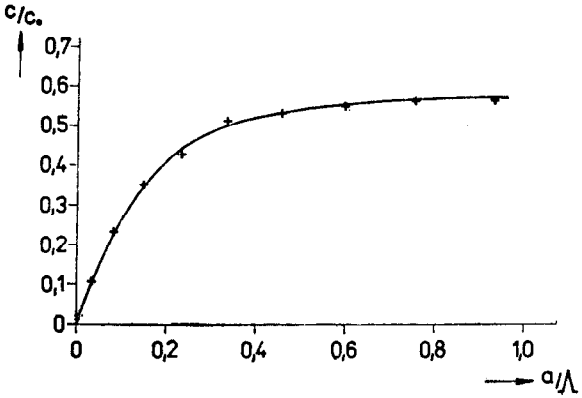

Fig. 4.

The values set up in Tab. IX are plotted in Fig. 4. The figure shows the particular points obtained by measuring the basic branch of the dispersion curve of flexural waves. Fig. 4 also shows the basic branch of the dispersion curve (solid line curve)

obtained by the Pochhammer equation for flexural waves ($\mu = 0{\cdot}29$) in a rod of infinite length. The differences being very small, it is evident that the influence of boundary conditions is not considerable.

3. NATURAL FREQUENCIES OF EXTENSIONAL VIBRATIONALS OF A THIN DISC

The disc of diameter $d_1 = 400$ mm, thickness $h = 12$ mm, made of structural carbon steel ($\mu = 0{\cdot}29$) was supported by three steel balls of diameter $d = 11$ mm. The balls were embedded in a plate, made of a plastic, in such a way that the positions of particular balls created an equilateral triangle, whose centrum was exactly below the centre of gravity of the disc (see Fig. 5). The embedding of the balls is shown in Fig. 6.

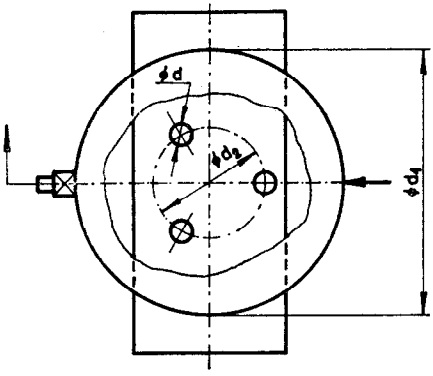

Fig. 5.

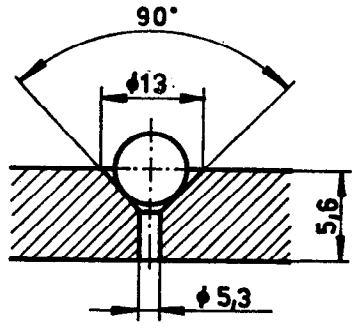

Fig. 6.

To study the influence of the embedding of the balls upon the spectrum of radial oscillations of the disc, three different magnitudes of the equilateral triangle of the embedding were used, namely three different diameters of the circumcircle of the equilateral triangle ($d_2 = 20$ mm, 100 mm, 160 mm) were chosen. It was found out that the magnitude of the diametre d_2 can only influence the damping of amplitudes of disc oscillations in time, whereas the values of frequencies remain practically unchanged.

Radial oscillations of extensional vibrations of a thin disc studied in [2]. Paper [4] presents the relations for calculation of natural radial frequencies of a thin disc:

(3-1) $$f_m = \frac{c_3 \beta_s}{2\pi r_1}$$ extensional vibration without components of circumferential displacements,

(3-2) $$f_m = \frac{c_3 \alpha_s^{(n)}}{2\pi r_1}$$ extensional vibration with components of circumferential displacements,

where c_3 stands for velocity of the dilatation wave in a two-dimensional continuum

(state of plane stress, for steel $c_3 = 5420\ \mathrm{m/s}$), r_1 is radius of the disc, constants (eigenvalues) β_s and $\alpha_s^{(n)}$ are given as positive roots of transcendental equations (23) and (24) in paper [2] (see also paper [5]). The eigenvalues of the disc in question are set up in Tab. X. The theoretical frequencies of extensional vibrations of the disc,

Table X

	$\mu = 0{\cdot}29$		
s	1	2	3
β_s	2·0425	—	—
$\alpha_s^{(1)}$	1·6248	3·5311	4·0712
$\alpha_s^{(2)}$	1·3974	2·5217	4·5378
$\alpha_s^{(3)}$	2·1448	3·4669	—
$\alpha_s^{(4)}$	2·7921	4·4217	—
$\alpha_s^{(5)}$	3·3989	—	—
$\alpha_s^{(6)}$	3·9860	—	—
$\alpha_s^{(7)}$	4·5619	—	—

Table XI

	$\mu = 0{\cdot}29$		
s	1	2	3
f_{mT} [Hz]	8 813	—	—
	7 011	15 236	17 566
	6 029	10 880	19 579
	9 254	14 958	—
	12 047	19 078	—
	14 665	—	—
	17 198	—	—
	19 683	—	—

obtained on substituting the values β_s, $\alpha_s^{(n)}$ into relations (3-1) and (3-2), are given in Tab. XI. As the maximum frequency range of the spectral analyzer B & K 2031 is 20 kHz, it follows from relations (3-1) and (3-2) that there is no use in considering the constants

(3-3) $$\beta_s > 4{\cdot}635\,, \quad \text{or} \quad \alpha_s^{(n)} > 4{\cdot}635\,.$$

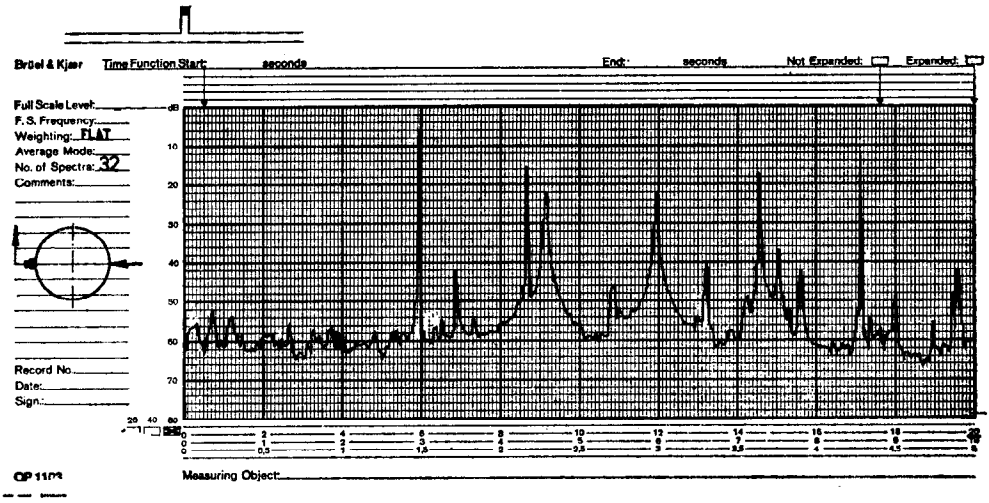

Fig. 7.

The spectrum of extensional vibrations of the disc, obtained by measuring, is shown in Fig. 7. This spectrum was obtained for $d_2 = 20$ mm (see Fig. 5).

The frequencies of the disc, f_m, obtained by measuring, are set up in Tab. XII.

Table XII

m	f_m [Hz]	f_{mT} [Hz]	$\lvert\Delta\rvert$ [%]
1	6 050	6 029	0·3
2	7 000	7 011	0·2
3	8 800	8 813	0·1
4	9 300	9 254	0·5
5	10 900	10 880	0·2
6	12 100	12 047	0·4
7	14 700	14 665	0·2
8	14 950	14 958	0·1
9	15 200	15 236	0·2
10	17 250	17 198	0·3
11	17 600	17 566	0·2
12	19 100	19 078	0·1
13	19 600	19 579	0·1
14	19 750	19 683	0·3

The table also shows the frequencies f_{mT} obtained by calculation (see Tab. XI), and also the absolute values of the percentage differences Δ between theoretical and experimental frequencies.

4. EIGENFREQUENCIES OF EXTENSIONAL VIBRATIONS OF A RING

4.1 Introductory remark

Let us consider the ring shown in Fig. 8. From the viewpoint of the theory of curved bars, this ring can be considered to be a thin ring if

$$R \geqq 10 \,.\, h\,, \tag{4-1}$$

where

$$R = \frac{D + d}{4} \tag{4-2}$$

is the medium radius of the ring.

Natural vibrations of a thin ring are treated in [1]. In general, the ring can experience either longitudinal or flexural vibrations. The flexural vibrations have the characteristic feature that their first natural frequency is considerably lower than that of oscillations arousing longitudinal deformation (only radial displacements).

Paper [6] presents the equation for calculation of angular frequencies of natural vibrations of a thin ring. This relation only little differs (in the region of low frequencies) from the well known Hoppe formulae (1874) which are as follows

$$(4\text{-}3)\quad \Omega_1^2 = \left(\frac{c_0}{R}\right)^2 (n^2 + 1) \qquad \text{for longitudinal vibrations,}$$

$$(4\text{-}4)\quad \Omega_2^2 = \left(\frac{c_0}{R}\right)^2 \left(\frac{j}{R}\right)^2 \frac{n^2(n^2 - 1)^2}{n^2 + 1} \qquad \text{for flexural vibrations } n = 0, 1, 2, \ldots,$$

j is a quadratic radius of inertia of the cross section of the ring.

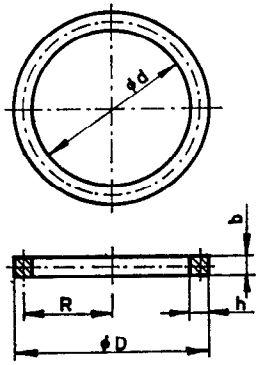

Fig. 8.

Paper [1] presents the derivation of natural frequencies of a thin ring via an improved theory respecting rotational inertia of the element, the influence of shearing forces and the influence of the transverse dimension of the ring (the Rayleigh correction respecting rotational inertia and the transverse dimension, the Timoshenko correction). This improved theory results in a cubic equation for calculation of eigenfrequencies. In view of the frequency range, which can be intercepted by the measuring arrangement, two smallest roots are of importance for the samples under consideration.

Vibrations of two different rings were investigated. The first ring was made from structural steel ($\mu = 0{\cdot}29$). Its dimensions are as follows (see Fig. 8):

$$\varnothing d = 280 \text{ mm}\,; \quad \varnothing D = 300 \text{ mm}\,; \quad b = h = 10 \text{ mm}\,.$$

The mean radius of the ring $R = 145$ mm. With reference to eq. (4-1), this ring can can be considered to be a thin ring.

The second ring was made from refined aloy structural steel ($\mu = 0{\cdot}30$). Its dimensions are as follows (see Fig. 8):

$$\varnothing d = 494 \text{ mm}\,; \quad \varnothing D = 566 \text{ mm}\,; \quad b = 16 \text{ mm}\,; \quad h = 36 \text{ mm}\,.$$

The mean radius of the ring $R = 265$ mm. With reference to eq. (4-1), this ring can be supposed to be a thick ring.

The spectra of eigenfrequencies of the above rings, obtained by measuring, were compared with theoretical spectra obtained via the following theories:

a) the frequency equation in paper [1], which results from the theory with corrections,

b) the frequency equation in paper [6], which follows from the theory without considering corrections,

c) the Hoppe formulae, see eq. (4-3), (4-4).

It ought to be remarked that all three above theories hold for vibrations of a thin ring. Nevertheles, these theories were intentionally employed for calculation of frequencies of thick ring too. This approach aimed at the experimental verification of applicability of the theories to a thick ring. It will be shown that the best results can be get through the theory with corrections.

4.2 Eigenfrequencies of a thin ring

The thin ring suspended on two threads (Fig. 9) was subjected to a mechanical impact.

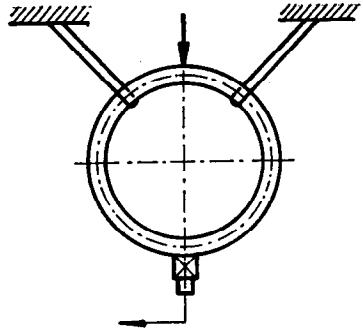

Fig. 9.

The spectrum of frequencies, obtained by measuring, is shown in Fig. 10.

The comparison of theoretical values of flexural frequencies with those obtained experimentally is given in Tab. XIII. The number n stands for the order of the eigenfrequency. The frequencies are non-zero for $n \geqq 2$. Symbol f_n refers to the values obtained by measuring, symbol f_{nP} stands for the values calculated via the theory with corrections, symbol f_{nM} represents the frequencies obtained through the theory without corrections, and symbol f_{nN} states the frequencies obtained by the Hoppe formulae. In Tab. XIII, the symbols $|\Delta_P|$, $|\Delta_M|$, $|\Delta_N|$ respectively stand for the absolute values of percentage differences between the theoretical values f_{nP}, f_{nM}, f_{nN} and experimental values f_n.

Tab. XIV shows the comparison of experimental values of longitudinal frequencies of the thin ring with theoretical values. The symbols used in this table are the same as those used in Tab. XIII.

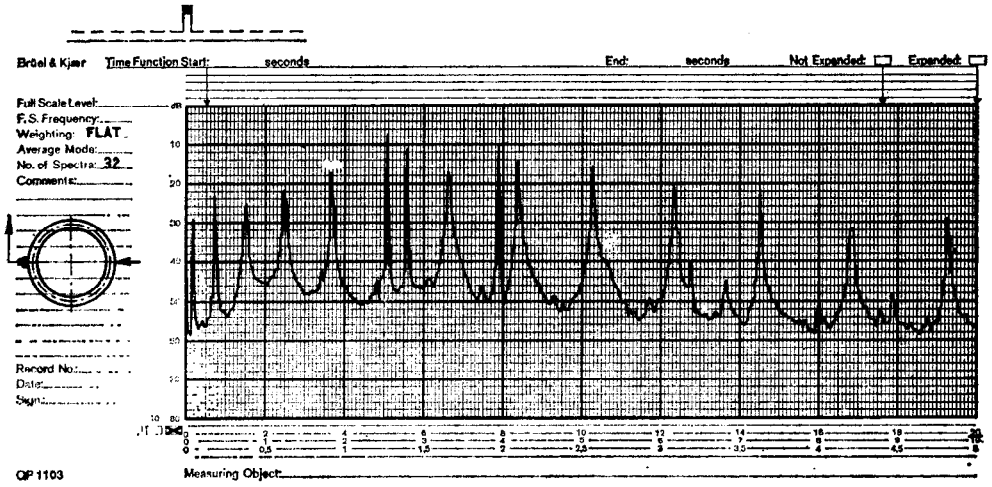

Fig. 10.

Table XIII

n	f_n [Hz]	f_{nP} [Hz]	$\lvert\Delta_P\rvert$ [%]	f_{nM} [Hz]	$\lvert\Delta_M\rvert$ [%]	f_{nN} [Hz]	$\lvert\Delta_N\rvert$ [%]
2	300	303	1·0	304	1·3	304	1·3
3	850	855	0·6	860	1·1	861	1·3
4	1 650	1 629	1·3	1 649	0·1	1 650	0·0
5	2 600	2 617	0·7	2 667	2·5	2 668	2·6
6	3 800	3 806	0·2	3 913	2·9	3 915	2·9
7	5 200	5 188	0·2	5 386	3·5	5 388	3·5
8	6 750	6 752	0·0	7 085	4·7	7 088	4·8
9	8 500	8 486	0·2	9 012	5·7	9 015	5·7
10	10 400	10 378	0·2	11 165	6·9	11 170	6·9
11	12 450	12 418	0·3	13 545	8·1	13 551	8·1
12	14 650	14 593	0·4	16 152	9·3	16 158	9·3
13	16 950	16 894	0·3	18 985	10·7	18 993	10·8
14	19 400	19 309	0·5	22 045	12·0	22 054	12·0

Table XIV

n	f_n [Hz]	f_{nP} [Hz]	$\lvert\Delta_P\rvert$ [%]	f_{nM} [Hz]	$\lvert\Delta_M\rvert$ [%]	f_{nN} [Hz]	$\lvert\Delta_N\rvert$ [%]
0	5 700	5 695	0·1	5 695	0·1	5 695	0·1
1	8 000	8 050	0·6	8 054	0·7	8 054	0·7
2	12 900	12 727	1·4	12 738	1·3	12 735	1·3
3	18 000	17 997	0·0	18 015	0·1	18 010	0·1

4.3 Eigenfrequencies of a thick ring

The thick ring was suspended on a copper wire of diameter 2 mm (see Fig. 11).

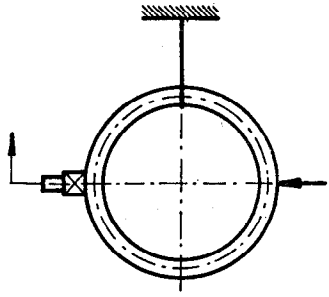

Fig. 11.

The spectrum of frequencies obtained by measuring is shown in Fig. 12.

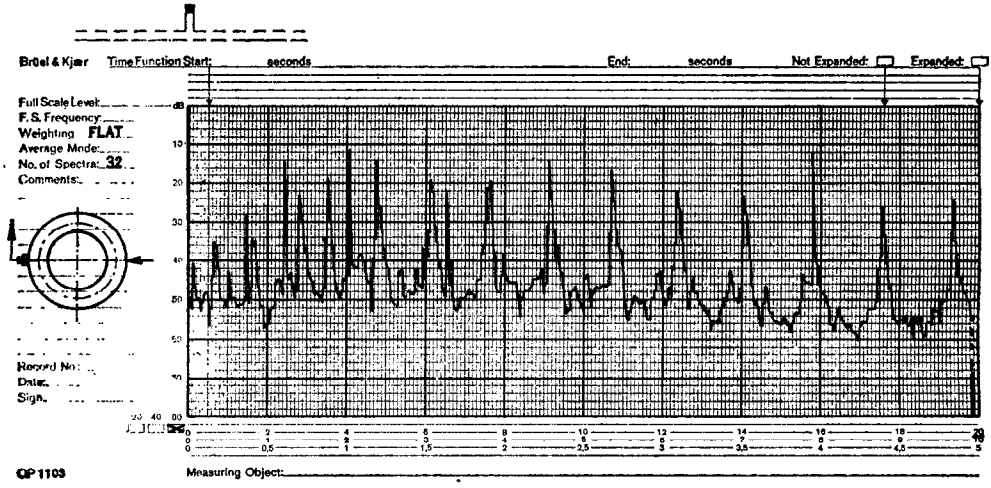

Fig. 12.

Tab. XV gives the comparison of the experimental values of flexural frequencies with theoretical values.

Tab. XVI refers to longitudinal frequencies of the thick ring.

The symbols used in Tabs. XV and XVI are the same as those in Tab. XIII.

Table XV

n	f_n [Hz]	f_{nP} [Hz]	$\lvert\Delta_P\rvert$ [%]	f_{nM} [Hz]	$\lvert\Delta_M\rvert$ [%]	f_{nN} [Hz]	$\lvert\Delta_N\rvert$ [%]
2	315	315	0·0	319	1·3	319	1·3
3	875	878	0·3	901	2·9	902	3·0
4	1 645	1 650	0·3	1 727	4·8	1 729	4·9
5	2 600	2 604	0·2	2 792	6·9	2 796	7·0
6	3 713	3 714	0·0	4 096	9·4	4 102	9·5
7	4 963	4 958	0·1	5 637	12·0	5 646	12·1
8	6 325	6 314	0·2	7 416	14·7	7 428	14·9
9	7 775	7 763	0·2	9 432	17·6	9 448	17·7
10	9 300	9 287	0·1	11 685	20·4	11 705	20·6
11	10 900	10 875	0·2	14 174	23·1	14 200	23·2
12	12 550	12 514	0·3	16 901	25·8	16 933	25·9
13	14 250	14 194	0·4	19 863	28·3	19 904	28·4
14	16 000	15 908	0·6	23 062	30·6	23 112	30·8
15	17 750	17 648	0·6	26 497	33·0	26 557	33·2
16	19 950	19 411	0·7	30 166	35·2	30 241	35·4

Table XVI

n	f_n [Hz]	f_{nP} [Hz]	$\lvert\Delta_P\rvert$ [%]	f_{nM} [Hz]	$\lvert\Delta_M\rvert$ [%]	f_{nN} [Hz]	$\lvert\Delta_N\rvert$ [%]
0	3 012	3 030	0·6	3 030	0·6	3 030	0·6
1	4 250	4 278	0·7	4 285	0·8	4 285	0·8
2	6 700	6 761	0·9	6 780	1·2	6 775	1·1
3	9 600	9 558	0·4	9 592	0·1	9 582	0·2
4	12 350	12 455	0·8	12 509	1·3	12 493	1·1
5	15 400	15 392	0·1	15 472	0·5	15 450	0·3
6	18 350	18 346	0·0	18 458	0·6	18 431	0·4

CONCLUSION

The paper contains the continuation of the previous authors' paper [3].

For a rod of circular cross section (cylindrical wave guide), the first three branches of dispersion characteristic of longitudinal rotationally symmetrical waves were obtained by measuring, including the basic branch of the dispersion characteristic of transversal waves. The particular points obtained by measuring are in a very good agreement with theoretical curves obtained for a rod of infinite length. Maximum errors for longitudinal and flexural waves respectively are 1·3% and 3·1%.

The analysis of eigenfrequencies of extensional vibration of a thin disc confirms correctness of the previous theories given in [2] and [5]. The maximum error between theoretical and experimental values ammounts to 0·5%.

The investigation of eigenfrequencies of extensional vibration of a thin ring confirmes exactness of the previous theory given in [1]. The best coincidence of results was obtained via the theory with corrections.

The results obtained by measuring the spectra of a thick ring show that the theory with corrections, originally developed for a thin ring, can be with high accuracy employed for calculations of natural spectra of a thick ring too.

The maximum errors between theoretical and experimental values attained through the improved theory are 1·4 or 0·9% for a thin and thick ring respectively. It turns out that the theory covers a fairly wide region, and can be, therefore, employed also for ratia $h/R > 0{\cdot}1$.

REFERENCES

[1] Brepta, R.: Investigation of properties of thin-wall shell models for solutions to stress wave propagation (In Czech), Research Report, Prague, ÚTAM ČSAV 1985.

[2] Brepta, R., Červ, J.: Thin elastic disc loaded by a sudden radial force. Acta Technica ČSAV, 1978, No. 3.

[3] Hégr, J.: Approximation and measurement of the basic branch of a dispersion curve of longitudinal rotationally symmetrical waves in circular cylindrical bars. Acta Technica ČSAV, 1986, No. 2.

[4] Hégr, J.: Electroacoustic impulse analysis of solid phase systems (In Czech), Thesis, Prague, ČVUT, Faculty of Electrical Engineering, 1986.

[5] Love, A. E. H.: Treatise on the mathematical theory of elasticity. Cambridge Press, 1927.

[6] Pajta, V., Půst, L.: Vibrations of slightly curved beams, (In Czech), Strojnický časopis SAV, 29, Bratislava 1978.

[Received March 3, 1987]

Doc. Ing. R. Brepta, DrSc., 162 00 Praha 6, Nad alejí 25, Ing. J. Hégr, CSc., 473 01 Nový Bor, 1. máje 341, Ing. P. Hora, 108 00 Praha 10, Nad vodojemem 52.